Am J Cancer Res 2023;13(9):3898-3920
www.ajcr.us /ISSN:2156-6976/ajcr0150957

Original Article

Bioinformatics analysis and experimental validation identified HMGA2/microRNA-200c-3p/LSAMP/Wnt axis as an immunological factor of patients with colorectal cancer

Xi Xu[1*], Chaoju Gong[2*], Yunfeng Wang[3], Zhidong Yin[1], Xiaogang Wang[1], Yanyan Hu[4], Zejun Fang[4]

[1]Department of Pathology, Second Affiliated Hospital, Zhejiang University School of Medicine, Hangzhou 310009, Zhejiang, China; [2]Central Laboratory, The Affiliated Xuzhou Municipal Hospital of Xuzhou Medical University, Xuzhou 221002, Jiangsu, China; [3]Department of Oncology, The First Affiliated Hospital of Zhengzhou University, Zhengzhou 450052, Henan, China; [4]Central Laboratory, Sanmen People's Hospital, Sanmen 317100, Zhejiang, China. [*]Equal contributors and co-first authors.

Received April 28, 2023; Accepted July 15, 2023; Epub September 15, 2023; Published September 30, 2023

Abstract: Colorectal cancer (CRC) is one of the most common malignant cancers. The tumor microenvironment (TME) plays an important role in tumor progression and affects the prognosis of CRC patients. However, the TME has been poorly characterized and studies aiming to identify the biomarkers or combined risk scores of CRC patients are limited. Here, we overlapped differentially expressed genes and stromal/immune-score-related modules to identify immune- and stromal-related genes in CRC patients. These genes were fed into the LASSO-Cox regression analysis for dimensionality reduction to establish a TME-associated risk model. A high TME-associated risk score was identified as an unfavorable prognostic factor in The Cancer Genome Atlas and Gene Expression Omnibus datasets, as well as in a subgroup analysis, stratified by gender, age, microsatellite instability, and tumor lymph node metastasis stage. Ten genes were mutated more frequently in the high TME-associated risk score group; these mutations may be related to changes in the TME and the response to immunotherapy. Thus, a lower TME-associated risk score may indicate a better response to immunotherapy and longer overall survival. Experimental validation demonstrated that *LSAMP*, a novel TME-associated-risk-score-related gene, increased sensitivity of CRC to $CD8^+$-T-cell-mediated cytotoxicity. A mechanistic investigation showed that the HMGA2/microRNA-200c-3p/LSAMP/Wnt axis was an immunological factor in CRC patients. To conclusion, we demonstrated that the TME-associated risk score model could be a reliable prognostic biomarker for CRC patients and highlighted the significance of the HMGA2/microRNA-200c-3p/LSAMP/Wnt axis in the oncoimmunology of CRC.

Keywords: HMGA2, microRNA-200c-3p, LSAMP, Wnt signaling, oncoimmunology, colorectal cancer

Introduction

Colorectal cancer (CRC) is one of the most common malignant cancers with the second highest mortality rate worldwide [1]. CRC patients diagnosed in the localized phase have a survival rate of approximately 80%, whereas the survival rate of CRC patients at the transfer phase is only ~20% [2]. Hence, identification of new potential biomarkers for diagnosis prediction will be beneficial to improving the prognosis of CRC patients.

During tumor progression, CRC cells and their surrounding environment constitute a specific tumor microenvironment (TME). Emerging studies have revealed that immune cells and stromal cells in the TME play an important role in tumor progression and could affect the prognosis of CRC patients [3-5]. Although some recent studies have focused on prognosis prediction based on TME in CRC [6-8], some limitations may affect the application for TME signature, including lacking real data for prospective analysis and verification, incomplete clinical infor-

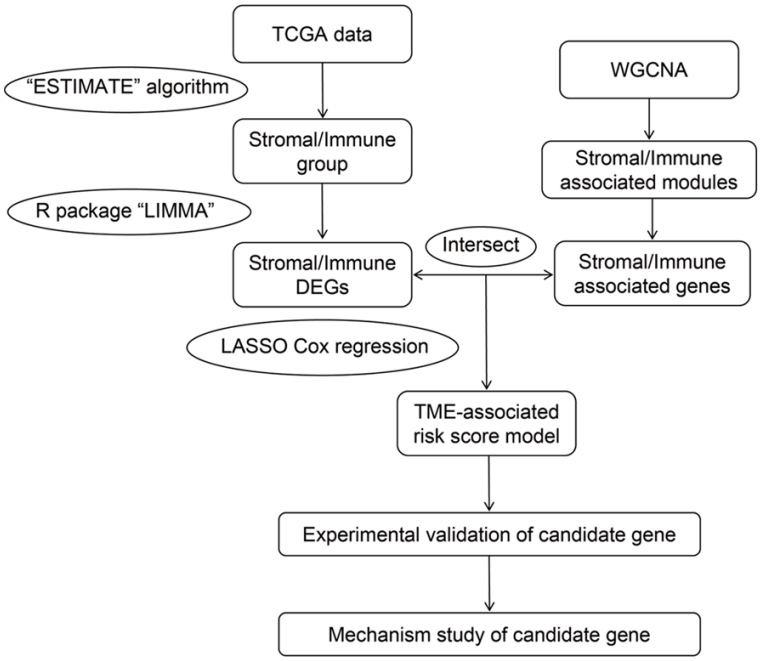

Figure 1. Flowchart of the present study.

mation of data, insufficient prediction accuracy. In addition, mechanism study for TME signature is also absent. Therefore, a better understanding of the TME and the identification of new biomarkers or combined risk scores is crucial to improving the prognosis of CRC patients.

In this study, we investigated the roles of TME-related genes in CRC and constructed a risk-score evaluation model to predict CRC prognosis. We found that the TME-associated risk score model could be constructed based on the expression of the following nine genes: HLX, WWTR1, LSAMP, PDGFRA, RAB3IL1, CRIP2, ADAM8, CCL22, and LGALS1. In addition, we investigated the role of LSAMP in oncoimmunology of CRC. Our mechanistic data identified high mobility group, AT-hook 2 (HMGA2)/microRNA-200c-3p as an upstream regulator of LSAMP, and LSAMP increased the sensitivity of CRC cells to $CD8^+$-T-cell-mediated cytotoxicity through blocking Wnt/β-catenin signaling. A flow diagram was provided in **Figure 1** to help understand the process of this study. Thus, we established a TME-associated risk model to predict CRC prognosis, while also highlighting the significance of the HMGA2/microRNA-200c-3p/LSAMP/Wnt axis in the oncoimmunology of CRC.

Materials and methods

Data sources and analysis methods used for calculating the immune and stromal scores

FPKM-normalized RNA-sequencing data were obtained from the Genomic Data Commons (GDC) Data Portal (https://portal.gdc.cancer.gov/). Clinical information of CRC patients was downloaded from GDC Data Portal (https://portal.gdc.cancer.gov/) and the UCSC Xena (https://xenabrowser.net/). Mutation data for CRC patients were obtained from UCSC Xena (https://xenabrowser.net/). Data relating to immune subtypes were generated in previous study [9]. The clinical characteristics of the CRC patients are shown in **Table 1**. Training datasets were downloaded from the GEO database; three GEO datasets (GSE30582, GSE87211, and GSE39582) were selected for further study.

DEG analysis and WGCNA

The R package "LIMMA" was used to identify DEGs; genes with $\log2|FC| \geq 1$ and FDR < 0.05 were identified as DEGs. The "WGCNA" R package was used to perform co-expression network analysis. Briefly, the expression level of a single gene was converted into a similarity matrix based on the Pearson correlation coefficient between paired genes. Outliers were detected using a hierarchical clustering tree, which was constructed using the expression matrix. According to the network topology analysis function, the scale-free topology fitting index was calculated as a function of the soft threshold power. Subsequently, a topological overlap dissimilarity measure (TOM) was used to calculate the intra-module connectivity between genes with similar expression profiles. Finally, a dynamic hybrid cutting method was used to divide these genes into different modules.

Table 1. Clinicopathological characteristics of CRC patients from The Cancer Genome Atlas dataset

Characteristic	Subtype	Number
MSI	Yes	14
	No	105
	NA	479
Pathologic_T	T1	18
	T2	103
	T3	409
	T4	65
	Tis	1
	NA	2
Pathologic_N	N0	337
	N1	146
	N2	111
	NX	2
	NA	2
Pathologic_M	M0	442
	M1	83
	MX	65
	NA	8
Stage	I	101
	II	217
	III	175
	IV	84
	NA	21
Immune_Subtype	C1	443
	C2	96
	C3	16
	C4	13
	C6	4
	NA	24
TCGA_Subtype	GI.CIN	311
	GI.GS	52
	GI.HM-indel	61
	GI.HM-SNV	9
	NA	156
OS	alive	475
	dead	123
Gender	female	274
	male	324

LASSO regularization and TME-related risk score calculation

LASSO is a linear regression method, which uses L1 regularization. L1 regularization reduces the weight of some learned features to zero for the purpose of sparsity and feature selection. The R software package "glmnet" was used to integrate survival time, survival status, and gene expression data; the LASSO-Cox method was then used for regression analysis. The risk score was calculated using the formula: TME-associated risk = $\sum \beta i * Expi$, where Expi represented the gene expression value and βi was the coefficient.

Analysis of tumor immune signatures and mutation status of the low- and high-TME-associated risk groups

The tumor immune signature, including infiltrating immune and stromal cells, was evaluated using the TIMER, CIBERSORT, and xCell algorithms. In the analysis of different mutation types, Frame_Shift_Del, Frame_Shift_Ins, In_Frame_Del, In_Frame_Ins, Missense, Nonsense, Nonstop, Splice_Site, and Translation_Start_Site were viewed as non-synonymous mutations. Silent mutations and other mutation types, including Intron, 3'-UTR, 5'-UTR, 3'-Flank, 5'-Flank, IGR, RNA, and Splice region, were considered as synonymous mutations; this type of mutation was regarded as wildtype (WT). Gene mutations that differed between the low- and high-TME-associated risk groups and their interactions were analyzed using the R package "Maftools".

Predicting the therapeutic sensitivity of patients with different TME-associated risk scores

We evaluated the predictive ability of the TME-associated risk score of the efficacy immunotherapy and 138 chemotherapeutic/targeted drugs. The 50% inhibiting concentration (IC50) value of 138 drugs was deduced using the pRRophic algorithm and the value was converted normally. The potential response of patients to immunotherapy was inferred from tumor immune dysfunction and rejection (TIDE) score and the immunophenotypic score (IPS).

Cell lines and cultures

The CRC cell lines, HCT116, SW620, and Rko, were purchased from the American Type Culture Collection (Rockville, USA) and cultured in RPMI 1640 (HyClone, Logan, UT, USA) supplemented with 10% fetal bovine serum

(Invitrogen). All cell lines were maintained in a 5% CO_2 atmosphere at 37°C.

Reagents and materials

RPMI 1640 medium was purchased from HyClone (Logan, UT, USA). Lipofectamine 3000 was obtained from Invitrogen (CA, USA). Secondary antibodies for western blotting were purchased from Li-COR Biosciences (NE, USA). The pcDNA3.1 plasmid containing full-length clone DNA of human LSAMP was obtained from Public Protein/Plasmid Library (Nanjing, China). The pCMV3 plasmid containing full length clone DNA of human HMGA2 was obtained from Sino Biological (Beijing, China). Small interfering RNAs (siRNAs) targeting human HMGA2 or LSAMP were purchased from GenePharma (Shanghai, China). Mimics of microRNA-200c-3p and negative control were purchased from GenePharma (Shanghai, China). All transfections were performed according to the manufacturer's instructions.

Western blotting

Total protein was obtained by lysing cells with RIPA lysis buffer. Nuclear and cytoplasmic proteins were obtained using the Nuclear and Cytoplasmic Protein Extraction Kit (Beyotime Biotechnology, Cat#P0027). The obtained protein lysates were heated for 5 min and resolved by sodium dodecyl-sulfate-polyacrylamide gel electrophoresis (SDS-PAGE) and transferred to nitrocellulose membranes. The following primary antibodies and dilutions were used: anti-LSAMP (1:1000, Bioss, Cat#bs-11091R), anti-β-catenin (1:1000, Cell Signaling Technology, Cat#8480), anti-β-tubulin (1:2000, Abcam, Cat#ab204947), anti-H3 (1:2000, Cell Signaling Technology, Cat#4499), and anti-GAPDH (1:8000, ProteinTech, Cat#60004-1-Ig).

Quantitative real-time PCR

Total RNA was extracted using the TRIzol method. Subsequently, quantitative real-time (qRT)-PCR was performed using reagents from TaKaRa, according to the manufacturer's manual. The gene transcripts were normalized to the transcript levels of the housekeeping gene GAPDH. The micro (mi)RNA level was examined using the Hairpin-it miRNA RT-PCR Quantitation Kit (GenePharma, Shanghai, China). We used U6 as the reference standard for normalizing miRNA expression. Three independent experiments were performed.

Apoptosis assay

CRC cells were cultured with TALL-104 cells at a ratio of 1:5, or alone, for 48 h. Then, the CRC cells were collected and resuspended in 200 μL binding buffer. Apoptosis assays were performed using the Annexin V-FITC/PI Apoptosis Kit (Multi Sciences, Cat#AP101) and analyzed by flow cytometry. Three independent experiments were performed.

Immunohistochemistry

Immunohistochemistry (IHC) was performed using an Envision Detection System (DAKO, USA) according to the manufacturer's instructions. IHC score evaluation was performed as previously described [10]. A 1:200 dilution of the anti-LSAMP primary antibody (Invitrogen, Cat#PA5-51223) and was used.

Lactate dehydrogenase assay

CRC cells were cultured with TALL-104 cells at a ratio of 1:5, or alone, for 48 h. Then, the cell culture plate was centrifuged and the CRC cell supernatant was aspirated as much as possible. Lactate dehydrogenase (LDH) released from CRC cells was detected using an LDH Cytotoxicity Test Kit (Beyotime Biotechnology, Cat#C0016) according to the manufacturer's instructions. Cytotoxicity (%) = (absorbance of treated samples - absorbance of samples in control well)/(absorbance of cells with maximum enzyme activity - absorbance of samples in control well) × 100. All of the experiments were repeated at least three times.

Dual luciferase reporter assay

HEK-293T cells were transfected with firefly luciferase reporter constructs and the control Renilla luciferase reporter pRL-TK using Lipofectamine 3000 (Invitrogen, CA, USA). After treatment, the cells were lysed with the cell lysis buffer provided in the Dual-Luciferase Reporter Assay Kit (Promega, USA, Cat#E1910). Luciferase activity was then measured according to the manufacturer's instructions. Three independent experiments were performed.

Chromatin immunoprecipitation (ChIP)

ChIP was performed as previously described. The primers used were used as follows: site 1: forward 5'-GTTGCAGCTGGGGCCACCCTC-3'; reverse 5'-GCAGCGGCCTGGATGAGGGGA-3'. site

2: forward 5'-GCCCTTATCCTCTTGGGCAG-3'; reverse 5'-CTGCCCAAGAGGATAAGGGC-3'. site 3: forward 5'-TCCCAAAGCCCAGAGGCTGG-3'; reverse 5'-GCTGTTCTCTCTCCCAGGCT-3'.

Immunofluorescence assay

CRC cells were seeded onto slides. 24 h later, the cells were fixed in 4% paraformaldehyde for 15 min at room temperature, washed three times with phosphate-buffered saline (PBS), then permeabilized with ice-cold 0.5% Triton X-100 for 20 min at room temperature, followed by three washes with PBS. The slides were blocked in PBS containing 10% bovine serum albumin for 30 min at room temperature, prior to being incubated with an anti-β-catenin antibody (1:100, Cell Signaling Technology, Cat# 8480) overnight at 4°C. After washing three times with PBS, the cells were incubated with an Alexa-Fluor-546-conjugated donkey anti-rabbit IgG (Invitrogen, Eugene, OR) for 1 h at room temperature in the dark. After three washes with PBS, DAPI (Zhongshan Goldenbridge Biotechnology Co., Ltd., Beijing, China) was used to stain the nuclei at room temperature for 10 min. The samples were stored at 4°C until being observed and photographed on a confocal microscope with image capture (LSM-510 Meta, Zeiss, Germany).

Statistical analysis

The Wilcoxon rank sum test was used for comparison of two groups and the Kruskal-Wallis rank sum test was used for comparison of multiple groups. Correlations were analyzed using the Pearson test. The Kaplan-Meier and log rank tests were used for survival analysis. For continuous variables, Cox regression was used to calculate the hazard ratio (HR) and the significance of differences in overall survival (OS). The correlations between expression levels and clinicopathologic parameters were determined using the χ^2 test. The permutation test was used for Gene Set Enrichment Analysis (GSEA). Analysis of differences between two groups was performed using a two-tailed Student's t-test and analysis of differences among mutiple groups was performed using analysis of variance (one-way with Tukey's post hoc test; two-way with Sidak's post hoc test). A *P*-value < 0.05 was considered as a measure of statistical significance. **P* < 0.05, ***P* < 0.01, ****P* < 0.001, *****P* < 0.0001.

Results

Calculation of immune/stromal scores and their correlation with the clinical features of CRC patients

We used the "ESTIMATE" algorithm to evaluate the extent of immune and stromal cell infiltration and generate stromal and immune scores. We then assessed the relationship between the stromal and immune scores and the pathological characteristics of the CRC patients. The results demonstrated that the immune score was higher than the stromal score in all subtypes of CRC (**Figure 2A**). CRC patients with higher levels of microsatellite instability (MSI) and those without metastasis or with lower-stage tumors had higher immune scores (**Figure 2B-D**). In addition, patients with advanced T stage tumors had higher stromal scores (**Figure 2E**). However, neither stromal score nor immune score correlated with tumor location, lymph node involvement, or gender (**Figure 2F-H**).

The cutoff value was determined by the "survminer" R package. The function of surv_cutpoint applies a sliding window process and eventually determines the best cutoff of -0.3077, which achieves the most significant statistical difference between the two groups. Subsequently, CRC patients were divided into high score and low score groups according to the optimized score threshold. The Kaplan-Meier and log rank tests were used in the survival analysis. The results illustrated that CRC patients with higher stromal or lower immune scores had a worse prognosis (**Figure 3A-D**). Furthermore, we used the "ESTIMATE" and "CPE" algorithms to evaluate the association between the stromal or immune score and tumor purity. We found that patients with a lower stromal score had higher tumor purity (**Figure 3E** and **3F**).

Calculation of the TME-associated risk score

DEGs between patients with high or low stromal/immune scores were identified using the R package "limma" with the threshold of FDR < 0.05 and |log2 (FC)| > log2 (1.5). A total of 1,204 stromal-score-related DEGs (1,079 genes were upregulated and 125 genes were downregulated) and 759 immune-score-related DEGs (739 genes were upregulated and 20

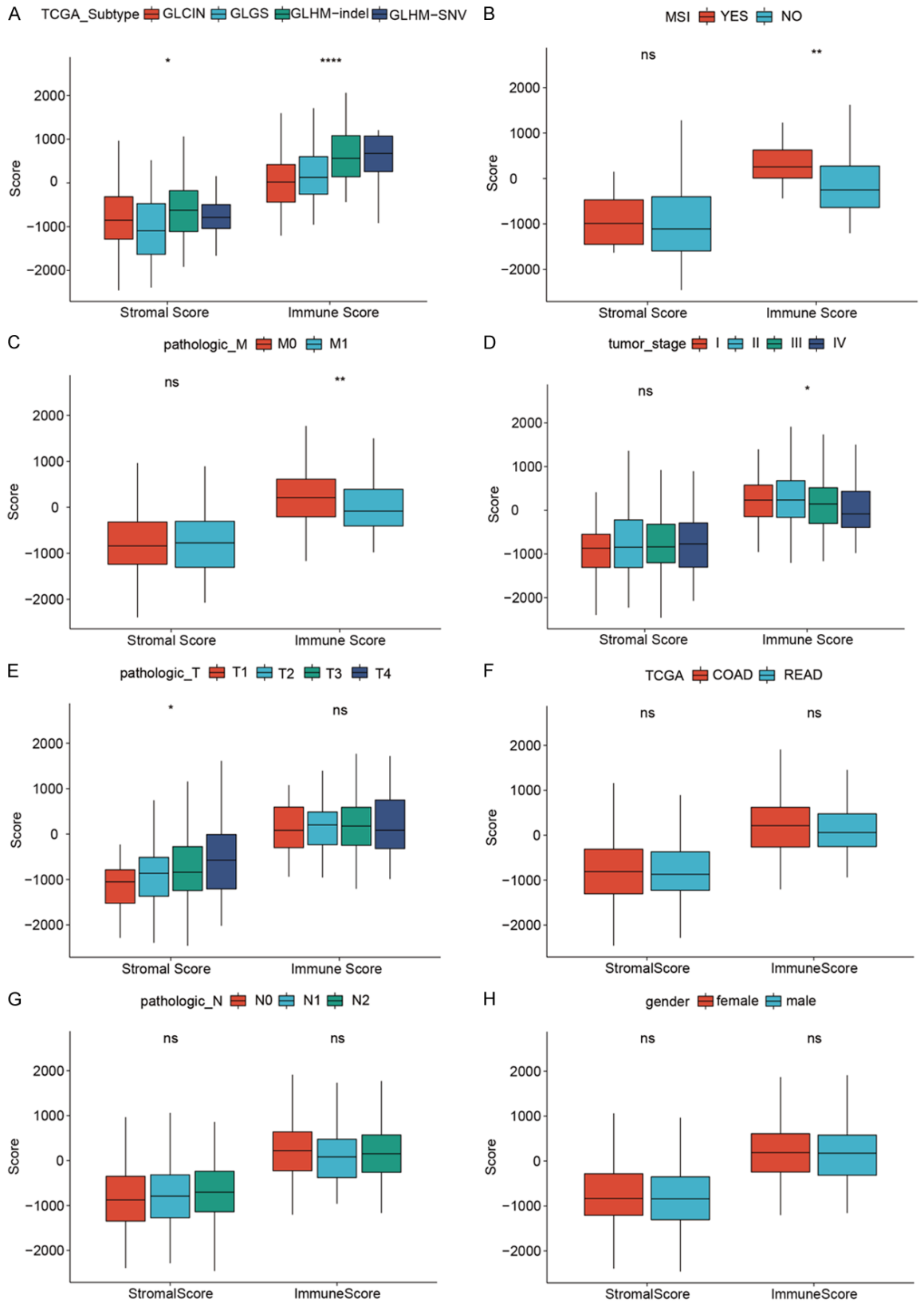

Figure 2. Association between stromal/immune scores and the clinicopathological characteristics of CRC patients. Distribution of (A) CRC subtypes, (B) microsatellites instability status, (C) metastasis status, (D) tumor stage, (E) T stage, (F) tumor location, (G) presence of lymph node metastasis, and (H) the gender of CRC patients among subgroups with different stromal/immune scores. *P < 0.05, **P < 0.01, ***P < 0.001, ****P < 0.0001.

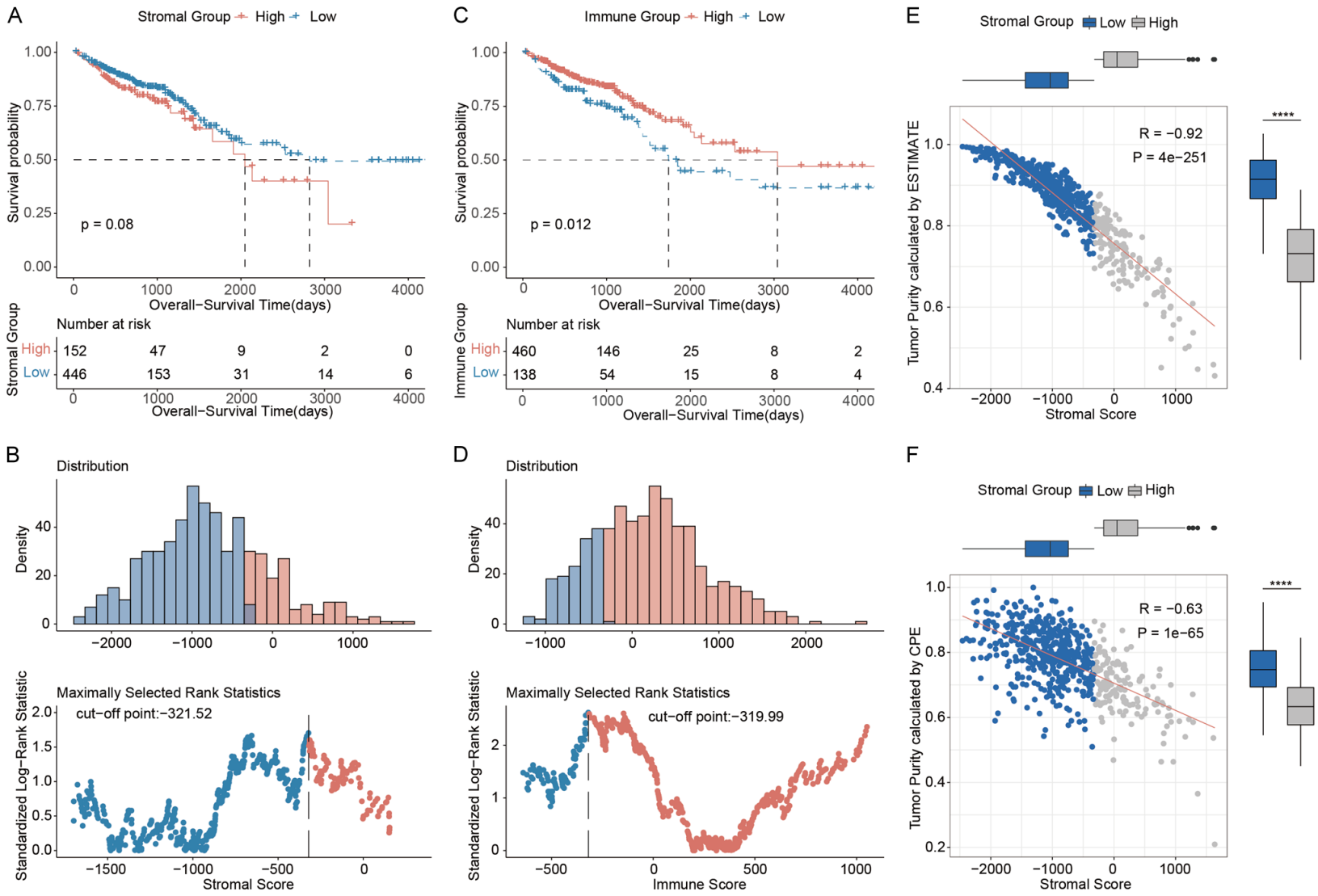

Figure 3. Association between stromal/immune scores and the prognosis of CRC patients. Survival analysis of CRC patients with low (A) or high (B) stromal scores. Survival analysis of CRC patients with low (C) or high (D) immune scores. The association between stromal scores and tumor purity, inferred by the (E) ESTIMATE and (F) CPE algorithms. *$P < 0.05$, **$P < 0.01$, ***$P < 0.001$, ****$P < 0.0001$.

genes were downregulated) were identified (data not shown).

We used the WGCNA package of R to identify stromal/immune-score-related modules. To achieve a scale-free topology, we selected an optimal soft threshold (β) of 14 and evaluated the connectivity of each gene (**Figure 4A**). We then split all genes into 20 parts according to their connectivity and calculated the average connectivity score of each part, the number of corresponding genes, and their correlation with the stromal/immune scores (**Figure 4B**). Finally, we used hybrid dynamic tree cut algorithm to set 30 as minimum gene number for each gene network module and generate 31 modules. In addition, the gray module represented a collection of uncorrelated genes (**Figure 4C**). Subsequently, candidate modules were selected if they significantly correlated with stromal/immune scores (i.e., $r > 0.5$, $P < 0.05$). Finally, a total of 20 modules were obtained. The results illustrated that red, black, blue, brown, and light yellow modules had a strong correlation with stromal score; while the red, blue, brown, and light yellow modules significantly correlated with the immune score (**Figure 4D**). We next overlapped the stromal/immune-score-related DEGs and the genes corresponding to the stromal/immune-score-related modules. 891 stromal-score-related DEGs and 534 immune-score-related DEGs were selected for further study (**Figure 4E** and **4F**). Then, these genes were fed into the LASSO-Cox regression analysis for dimensionality reduction (**Figure 4G** and **4H**).

Next, we included the gene union list obtained from LASSO Cox regression dimensionality reduction in the stepwise regression analysis (based on multivariate Cox regression analysis). The model, which comprised HLX, WWTR1, LSAMP, PDGFRA, RAB3IL1, CRIP2, ADAM8, CCL22, and LGALS1, had a minimum Akaike information criterion (AIC) value of 1,320.39 (**Figure 4I**). In the final risk model, TME-associated risk was calculated as follows: TME-associated risk = 0.9687 × HLX + 0.3041 × WWTR1 - 0.5553 × LSAMP - 0.3457 × PDGFRA + 0.3923 × RAB3IL1 + 0.2739 × CRIP2 + 0.2863 × ADAM8 - 0.5885 × CCL22 - 0.4231 × LGALS1. According to the TME-associated risk score of each sample, patients were divided into high- and low-risk groups. Kaplan-Meier analysis was used to calculate the survival of each group, which were then compared using the log rank test. The results demonstrated that in the GSE87211 and GSE39582 cohorts, and the TCGA-colon adenocarcinoma (COAD) dataset, CRC patients with higher TME-associated risk scores had shorter survival times (**Figure 5A-E**). Furthermore, the time-dependent area under the receiver operating characteristic (ROC) curve (AUC) illustrated that the TME-associated risk score was a predictive factor for OS of CRC patients in the TCGA and GEO datasets (**Figure 5F**). Moreover, the combination of TME-associated risk and tumor lymph node metastasis (TNM) significantly increased the C-statistic for survival prediction in both the TCGA and GSE30582 cohorts (**Figure 5G**).

Correlation analysis of the TME-associated risk score with clinicopathological features and immune signature

To evaluate whether the TME-associated risk score acted as an independent risk factor for CRC, Cox regression analysis was used. The results demonstrated that the TME-associated risk score was an independent risk factor for the OS of CRC patients in the TCGA cohort (**Figure 5H**).

Next, the correlations between the TME-associated risk score and the clinicopathological features of CRC patients were investigated. We found that the TME-associated risk score varied between patients with different CRC subtypes (**Figure 6A**). For instance, patients with MSI had lower TME-associated risk scores (**Figure 6B**) and that TME-associated risk score positively correlated with tumor size, adjacent tissue involvement, lymph node metastasis, organic metastasis, and tumor stage (**Figure 6C-F**). However, no significant correlation was observed between the TME-associated risk score and gender or tumor location (**Figure 6G** and **6H**).

In addition, we used TIMER, CIBERSORT, and xCell to investigate the distribution of infiltrating immune cells in low and high TME-associated risk groups of CRC patients. Our results demonstrated that CRC patients with high TME-associated risk scores tended to have lower numbers of infiltrating immune or stromal cells (**Figure 7A**). We also analyzed the prognostic values of immune cell infiltrates in

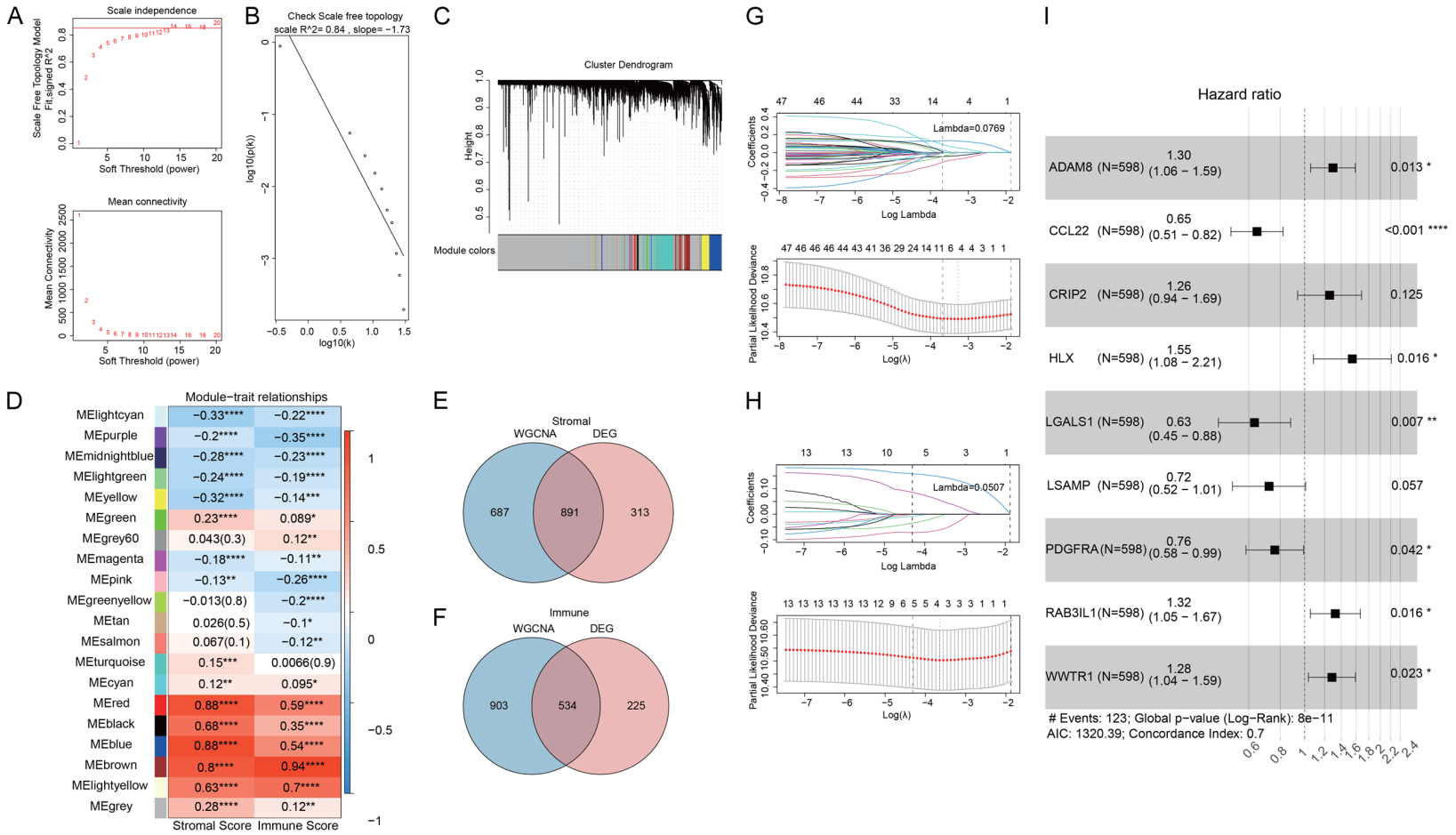

Figure 4. Construction of the TME-associated risk score model. A. Determination of the adjacency function β parameter in the weighted gene co-expression network analysis algorithm. B. Connectivity distribution evaluation. C. The gene modules identified by WGCNA. D. The correlation between gene modules and immune/stromal scores. E. A Venn diagram showing the number of intersecting genes derived from the stromal-score-associated DEG analysis and WGCNA. F. A Venn diagram showing the number of intersecting genes derived from the immune-score-associated DEG analysis and WGCNA. G. LASSO regression for the dimension reduction of stroma-associated, prognosis-related genes. Cross-validation in the LASSO regression model to select the tuning parameter. The abscissa shows the log (λ) value, and the ordinate shows partial likelihood deviance. The red dots in the figure show partial likelihood deviations ± standard error for diverse tuning parameters. H. LASSO regression for the dimension reduction of immune-associated, prognosis-related genes. Cross-validation in the LASSO regression model to select the tuning parameter. The abscissa shows the log (λ) value, and the ordinate shows partial likelihood deviance. The red dots in the figure show partial likelihood deviations ± standard error for diverse tuning parameters. I. Multivariable Cox regression analysis revealed nine prognosis-related genes in CRC patients. *$P < 0.05$, **$P < 0.01$, ***$P < 0.001$.

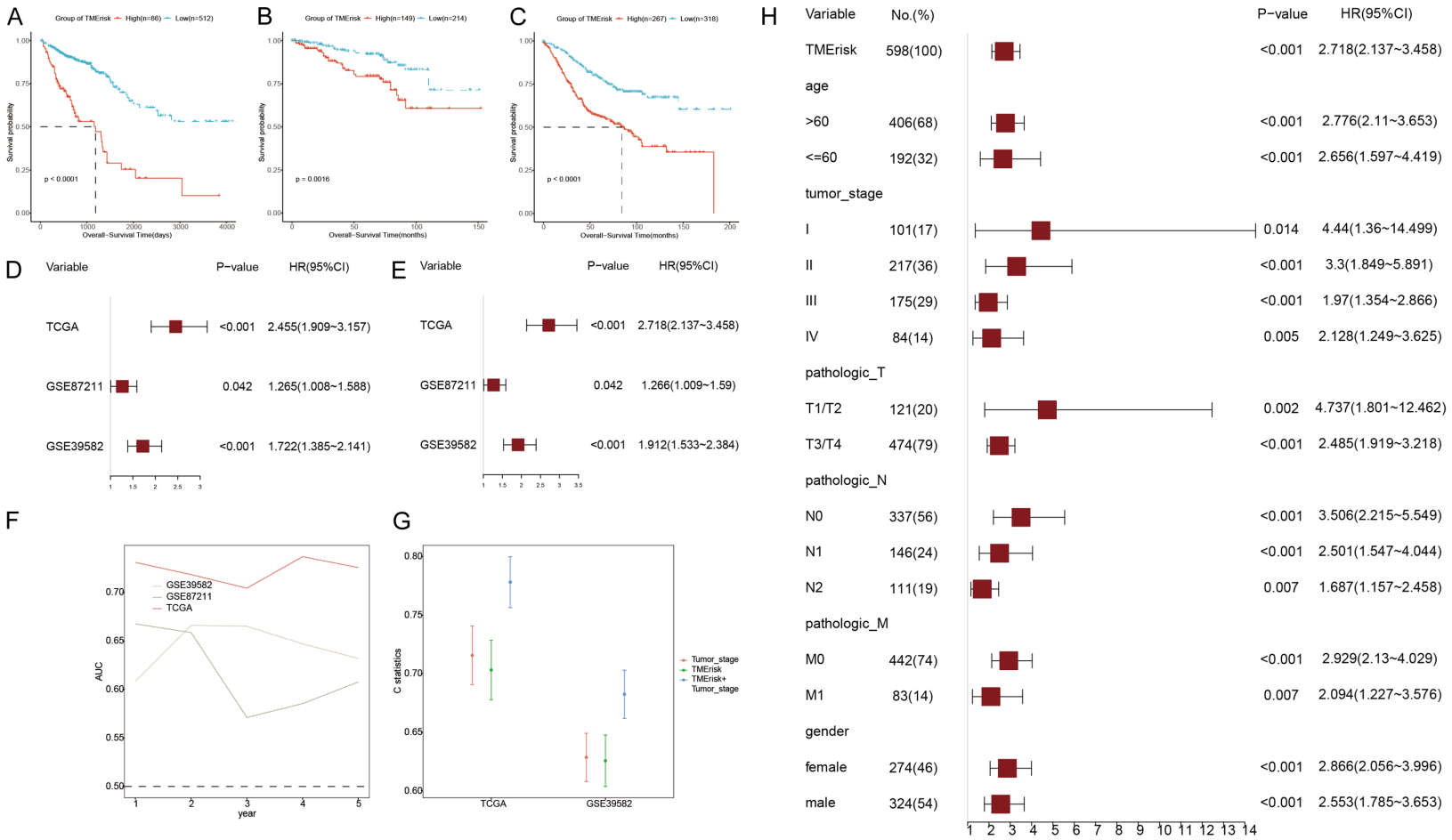

Figure 5. Prognostic value of the TME-associated risk score in CRC patients. The association between the TME-associated risk score and the overall survival (OS) of CRC patients from the (A) TCGA-COAD, (B) GSE87211, and (C) GSE39582 cohorts. Forest plot of the (D) multivariate Cox analysis and the (E) univariate Cox analysis of the TCGA and GEO datasets. (F) Time-dependent AUC value for the TCGA and GEO datasets. (G) The C-statistics of tumor stage and TME-associated risk for the TCGA and GEO datasets. (H) Stratified analysis suggested that groups of CRC patients with low or high TME-associated risk scores and different clinicopathological characteristics had significant differences in OS.

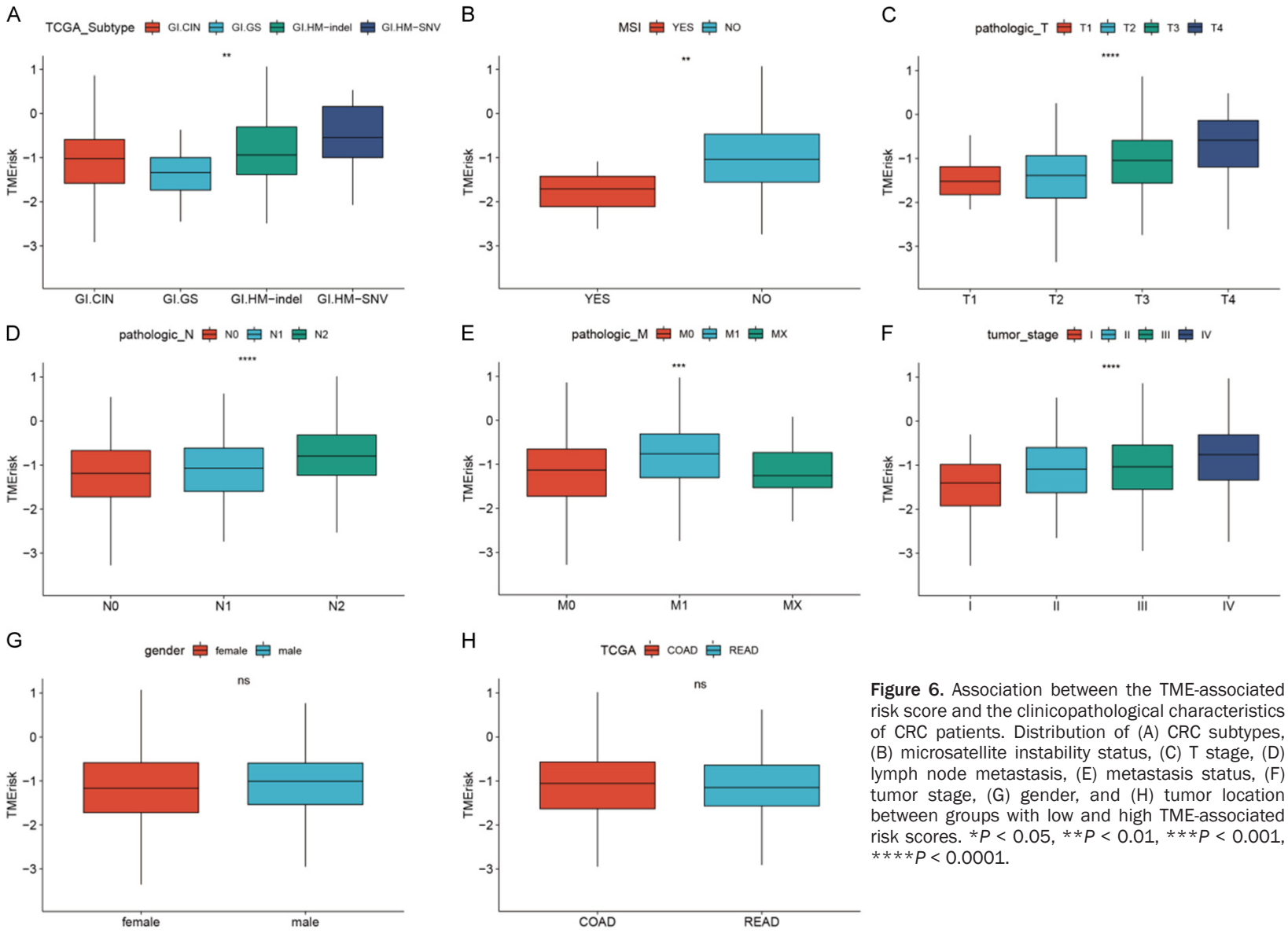

Figure 6. Association between the TME-associated risk score and the clinicopathological characteristics of CRC patients. Distribution of (A) CRC subtypes, (B) microsatellite instability status, (C) T stage, (D) lymph node metastasis, (E) metastasis status, (F) tumor stage, (G) gender, and (H) tumor location between groups with low and high TME-associated risk scores. **P* < 0.05, ***P* < 0.01, ****P* < 0.001, *****P* < 0.0001.

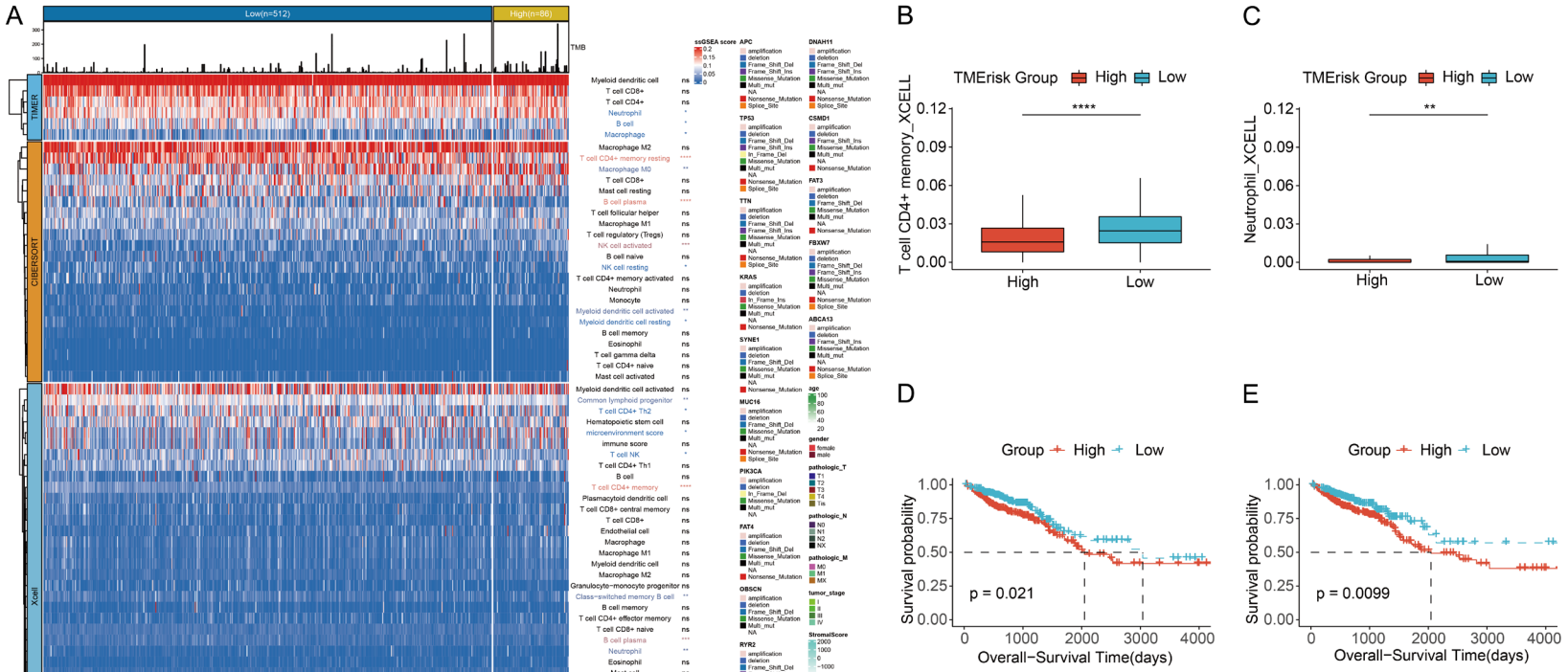

Figure 7. Association between the TME-associated risk scores and immune signatures of CRC patients. (A) Landscape of immune and stromal cell infiltrations in the groups with low or high TME-associated risk scores. Distribution of (B) $CD4^+$ memory T cell and (C) neutrophils between the groups with low or high TME-associated risk scores. Impact of (D) $CD4^+$ memory T cell and (E) neutrophil infiltrations on CRC patient prognosis. $*P < 0.05$, $**P < 0.01$, $***P < 0.001$, $****P < 0.0001$.

the low and high TME-associated risk groups. The results demonstrated that the numbers of infiltrating $CD4^+$ memory T cells and neutrophils were lower in the high TME-associated risk group (**Figure 7B** and **7D**). However, patients with higher TME-associated risk scores had shorter OS, despite higher numbers of infiltrating $CD4^+$ memory T cells or neutrophils (**Figure 7C** and **7E**).

Mutation status of CRC patients in the high and low TME-associated risk groups

To study the mechanism underlying TME-associated risk, we investigated somatic mutations using TCGA data. When comparing the mutation frequencies between low and high TME-associated risk groups, we found that the high TME-associated risk group had more somatic mutations than the low-risk group, including non-synonymous and synonymous mutations (Supplementary Figure 1A-C).

Genes with mutation frequencies over 30 in either the low or the high TME-associated risk group were labelled as high mutation frequency genes. We found ten high mutation frequency genes, including USH2A, DNAH7, NEB, DOCK2, WDR87, LRRIQ1, CACNA1C, UGGT2, ABCB1, and BCLAF1 had prognostic efficacy. With the exception of ABCB1, all these genes were prognostic risk factors for mutation status in CRC patients (Supplementary Figure 1D); the frequency of mutations in these genes was shown in **Figure 7A**. Co-mutation analysis illustrated obvious co-mutations among these genes and revealed that the high TME-associated risk group had more co-mutations. In addition, ABCB1 significantly co-mutated with the other nine genes and the mutation rate of ABCB1 was higher in the high TME-associated risk group (Supplementary Figure 1E and 1F).

TME-associated risk predicts therapeutic benefits

We next investigated whether TME-associated risk could be used as a biomarker to predict the drug response (including to chemotherapy, targeted therapy, and immunotherapy) in patients with CRC. We found that CRC patients with high TME-associated risk might be more sensitive to drug therapy (**Figure 8A**). Besides, patients with lower TME-associated risk scores had lower TIDE scores, indicating that patients with lower TME-associated risk scores may respond better to immunotherapy (**Figure 8B** and **8C**).

LSAMP, a novel TME-associated-risk-score-related gene, facilitates sensitivity to $CD8^+$-T-cell-mediated cytotoxicity

The immunosuppressive TME contributes to cancer immune escape. Thus, we sought to explore the biological functions of the identified TME-associated-risk-score-related genes. Among the nine genes identified, a novel TME-associated-risk-score-related gene, *LSAMP*, drew our attention. Although a recent study demonstrated *LSAMP* was involved in a prognostic risk-scoring model based on sphingolipid metabolism-associated cluster in CRC [11], there hasn't been any study indicating a causal relationship between the gene of *LSAMP* and the oncoimmunology of CRC. What's more, **Figure 4I** illustrated that among the 9 indicators, *LSAMP* is considered protective factor with a hazard ratio of 0.72. It suggests a potential relationship between the expression of *LSAMP* and a favorable prognosis of CRC. Hence, a series of validation experiments was exploited to illustrate the relation between *LSAMP* and the oncoimmunology of CRC.

IHC analysis showed non-tumor tissues expressed high levels of LSAMP (**Figure 9A**). Moreover, survival analysis showed that CRC patients with high *LSAMP* expression were more likely have a significantly longer OS than the those in the other groups (P = 0.031; **Figure 9B**). Several clinicopathological parameters were demonstrated to be significantly correlated with LSAMP expression. High LSAMP expression was negatively correlated with lymph node metastasis (95% CI: 0.1887-0.9348, P = 0.032), TNM stage (95% CI: 0.1947-0.9781, P = 0.042), and distant metastasis (95% CI: 0.1625-0.8320, P = 0.015) (**Table 2**).

Subsequently, we examined expression level of *LSAMP* in different CRC cell lines and found that it was more highly expressed in HCT116 and Rko cells and less expressed in SW620 cells (**Figure 9C**). Therefore, we overexpressed *LSAMP* in SW620 cells and knocked down its expression in HCT116 cells (**Figure 9D**). To evaluate the effect of LSAMP on cancer immune evasion, CRC cells were co-cultured with a

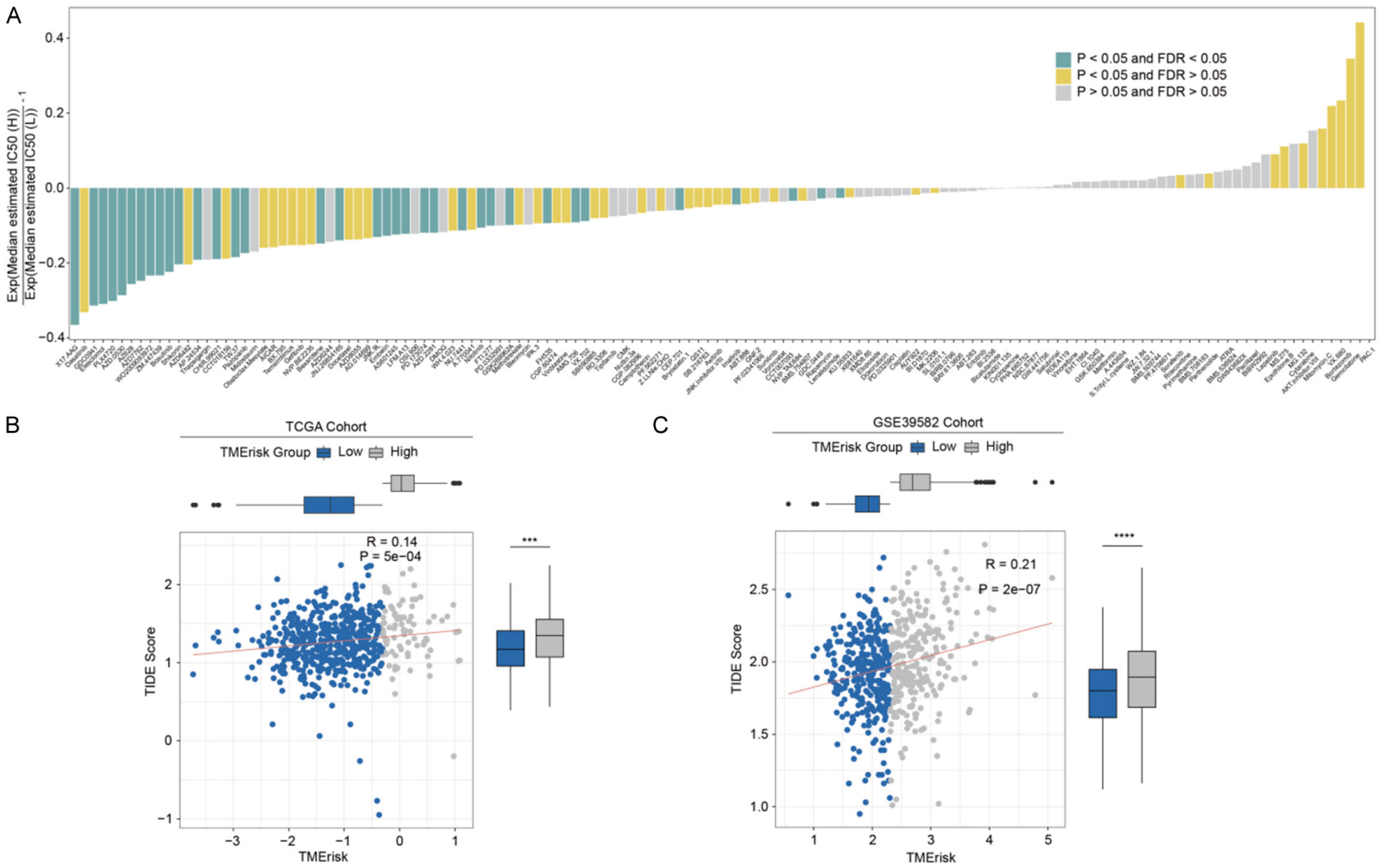

Figure 8. Association between the TME-associated risk score and therapeutic efficiency. (A) Ratio of normalized IC50 value of the 138 drugs between the low-risk and high-risk groups. Distribution of TIDE scores in the low or high TME-associated risk score groups of the (B) TCGA and (C) GSE39582 cohorts. ***$P < 0.001$, ****$P < 0.0001$.

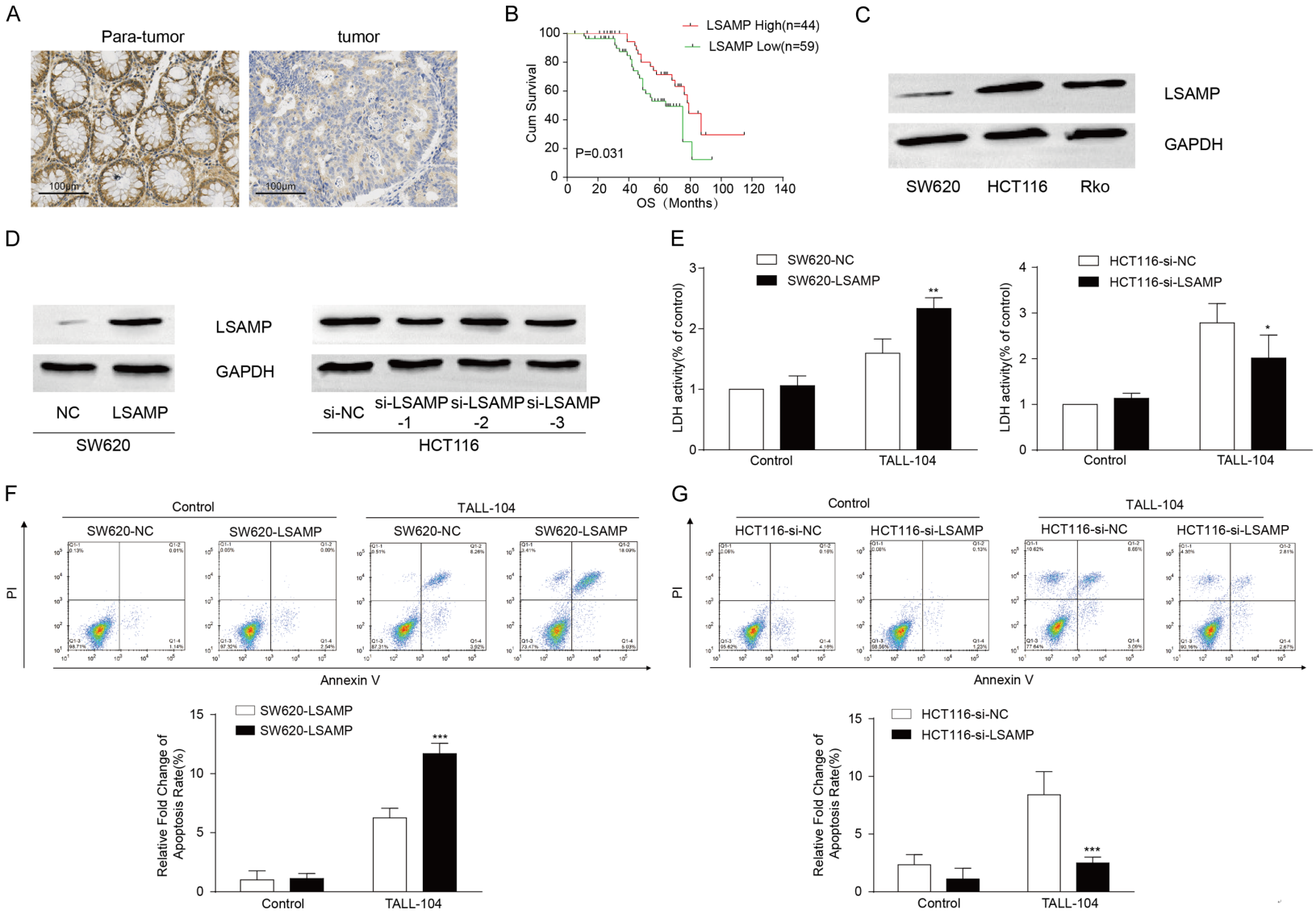

Figure 9. LSAMP increases the sensitivity of CRC cells to CD8⁺-T-cell-mediated cytotoxicity. A. Immunohistochemistry staining for LSAMP in CRC samples and adjacent normal tissues. B. OS analysis of CRC patients with high or low levels of *LSAMP*. C. LSAMP expression in CRC cell lines. D. Overexpression and knockdown of *LSAMP* in SW620 and HCT116 cells, respectively. E. Results of an LDH cytotoxicity assay involving SW620-NC/LSAMP cells or HCT116-si-NC/si-LSAMP cells in the presence of absence of TALL-104 cells. F. Flow cytometry analysis of SW620-NC/LSAMP cell apoptosis in the presence or absence of TALL-104 cells. G. Flow cytometry analysis of HCT116-si-NC/si-LSAMP apoptosis in the presence of absence of TALL-104 cells. $^{*}P < 0.05$, $^{**}P < 0.01$, $^{***}P < 0.001$.

Table 2. Relationship between LSAMP expression and the clinicopathological characteristics of CRC patients

	LSAMP expression		
	Low	High	
	Cases	Cases	*P* Value
	59	44	
Tumor location			0.754
Colon	29	23	
Rectum	30	21	
Gender			0.975
Male	27	20	
Female	32	24	
Age			0.882
≤ 65	34	26	
> 65	25	18	
Tumor size			0.260
< 5 cm	28	16	
≥ 5 cm	31	28	
LNM			0.032*
N0	21	25	
N1/2	38	19	
TNM			0.042*
I/II	27	29	
III/IV	32	15	
Distant metastasis			0.015*
M0	26	30	
M1	33	14	

*$P < 0.05$.

human cytotoxic $CD8^+$ T cell line, TALL-104. The results demonstrated that LSAMP attenuated CRC resistance to $CD8^+$-T-cell-mediated cytotoxicity (**Figure 9E**). In addition, LSAMP reduced survival rate of CRC cells co-cultured with TALL-104 cells (**Figure 9F** and **9G**). Overall, these results illustrated that the knockdown of *LSAMP* expression correlated with an immunosuppressive phenotype in CRC.

LSAMP increases the sensitivity of CRC cells to $CD8^+$-T-cell-mediated cytotoxicity by blocking Wnt/β-catenin signaling

Aberrant Wnt/β-catenin signaling plays a vital role in the metastasis, proliferation, and immune evasion of CRC [12-14]. Thus, we sought to investigate whether LSAMP regulated sensitivity to $CD8^+$-T-cell-mediated cytotoxicity via Wnt/β-catenin signaling. GSEA showed that the Wnt pathway strongly negatively associated with LSAMP expression (NES = -1.47; P = 0.014) (**Figure 10A**). The TOP/FOP flash dual-luciferase assay showed that knockdown of LSAMP significantly increased the transcriptional activity of the canonical Wnt reporter (**Figure 10B**). Nuclear translocation of β-catenin is an important prerequisite for the activation of downstream transcription factors. Western blotting and immunofluorescence revealed that the nuclear localization of β-catenin was attenuated by LSAMP expression (**Figure 10C** and **10D**). Collectively, these results demonstrate that LSAMP inhibited Wnt/β-catenin signaling.

To further explore the involvement of Wnt/β-catenin signaling in LSAMP-mediated sensitivity to $CD8^+$-T-cell-mediated cytotoxicity, we exploited SKL2001, an activator of β-catenin and thereby activating the Wnt signaling pathway [15], to carry out rescue experiments. The results showed that sensitivity to $CD8^+$-T-cell-mediated cytotoxicity was hindered by SKL2001 treatment in LSAMP-overexpressing cells compared with control cells (**Figure 10E**). This result firmly indicates that LSAMP increased the sensitivity of CRC cells to $CD8^+$-T-cell-mediated cytotoxicity by suppressing Wnt/β-catenin signaling.

HMGA2 promotes an immunosuppressive phenotype in CRC via the miRNA-200c-3p/LSAMP/Wnt/β-catenin axis

The aforementioned results indicate that LSAMP negatively correlates with TME risk of CRC. However, the mechanism underlying the regulation of LSAMP expression in CRC remained unknown. As an important regulatory molecule of target gene-expression, miRNA is closely related to CRC tumorigenesis. Therefore, we hypothesized that miRNA accounted for differences in LSAMP expression. We used TargetScan, a database for predicting miRNA binding sites, to screen for candidate regulators of LSAMP. The prediction results demonstrated that the 3'-UTR of *LSAMP* contained putative complementary binding sites for miRNA-200c-3p (**Figure 11A**). Western blotting was then used to demonstrate that blocking miRNA-200c-3p induced LSAMP expression (**Figure 11B**). Subsequently, HEK293T cells were transfected with miRNA-200c-3p mimics and the luciferase reporter vector containing the WT or mutant 3'-UTR of *LSAMP*. The results demonstrated that the overexpression of miRNA-200c-3p significantly decreased the luciferase activity of cells expressing the WT

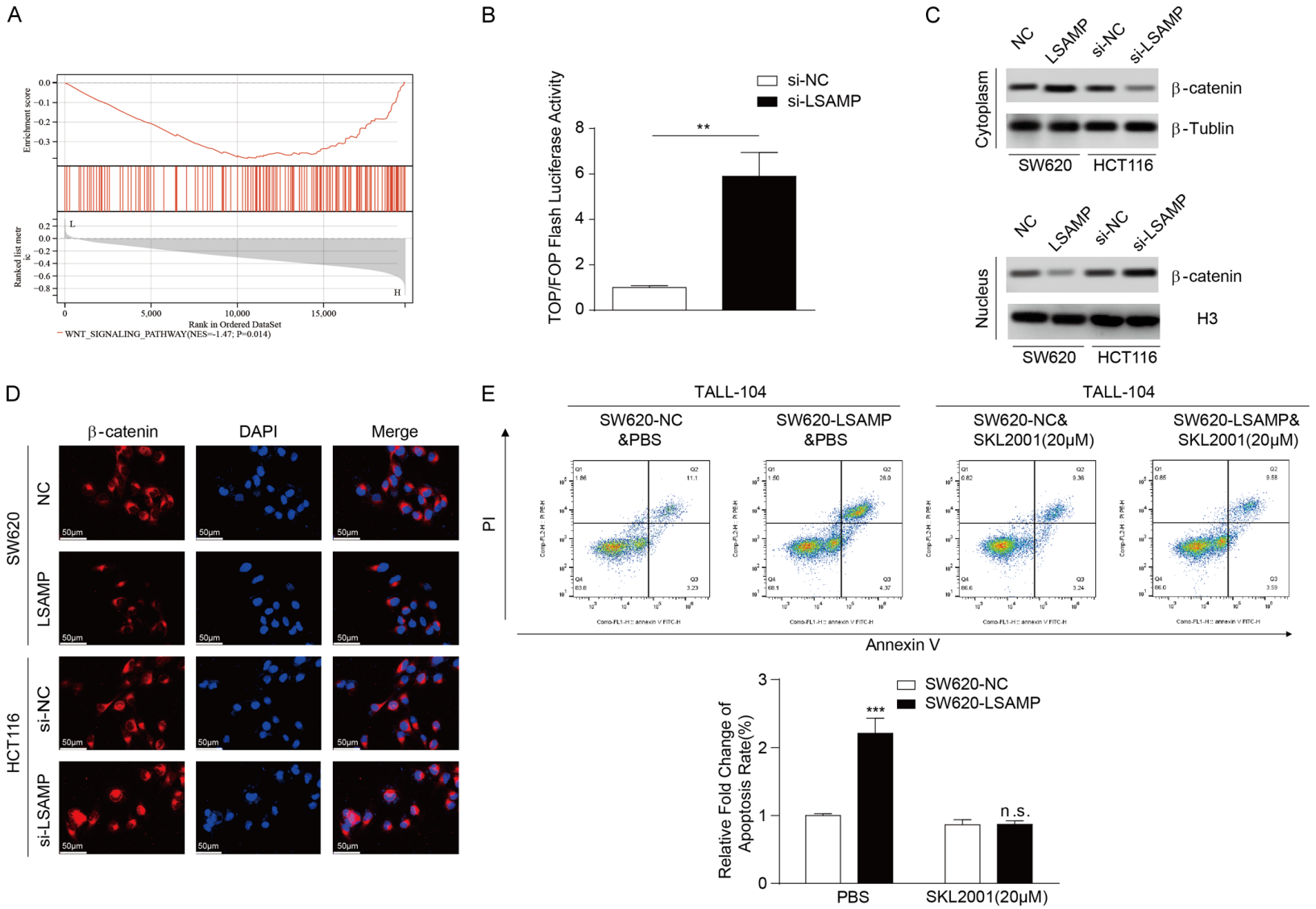

Figure 10. LSAMP increases the sensitivity of CRC cells to $CD8^+$-T-cell-mediated cytotoxicity by blocking Wnt/β-catenin signaling. (A) GSEA illustrated a strong association between the Wnt pathway and LSAMP expression. (B) The luciferase activity assay showed that silencing *LSAMP* significantly increased the ratio of TOP Flash to FOP Flash activity in the HCT116 cell line. (C) Western blotting and (D) immunofluorescence showed that the nuclear localization of β-catenin was attenuated by LSAMP. (E) Flow cytometry analysis of apoptosis was performed in SKL2001-treated or untreated SW620-NC/LSAMP cells as well as in the presence of TALL-104 cells. $^{**}P < 0.01$, $^{***}P < 0.001$.

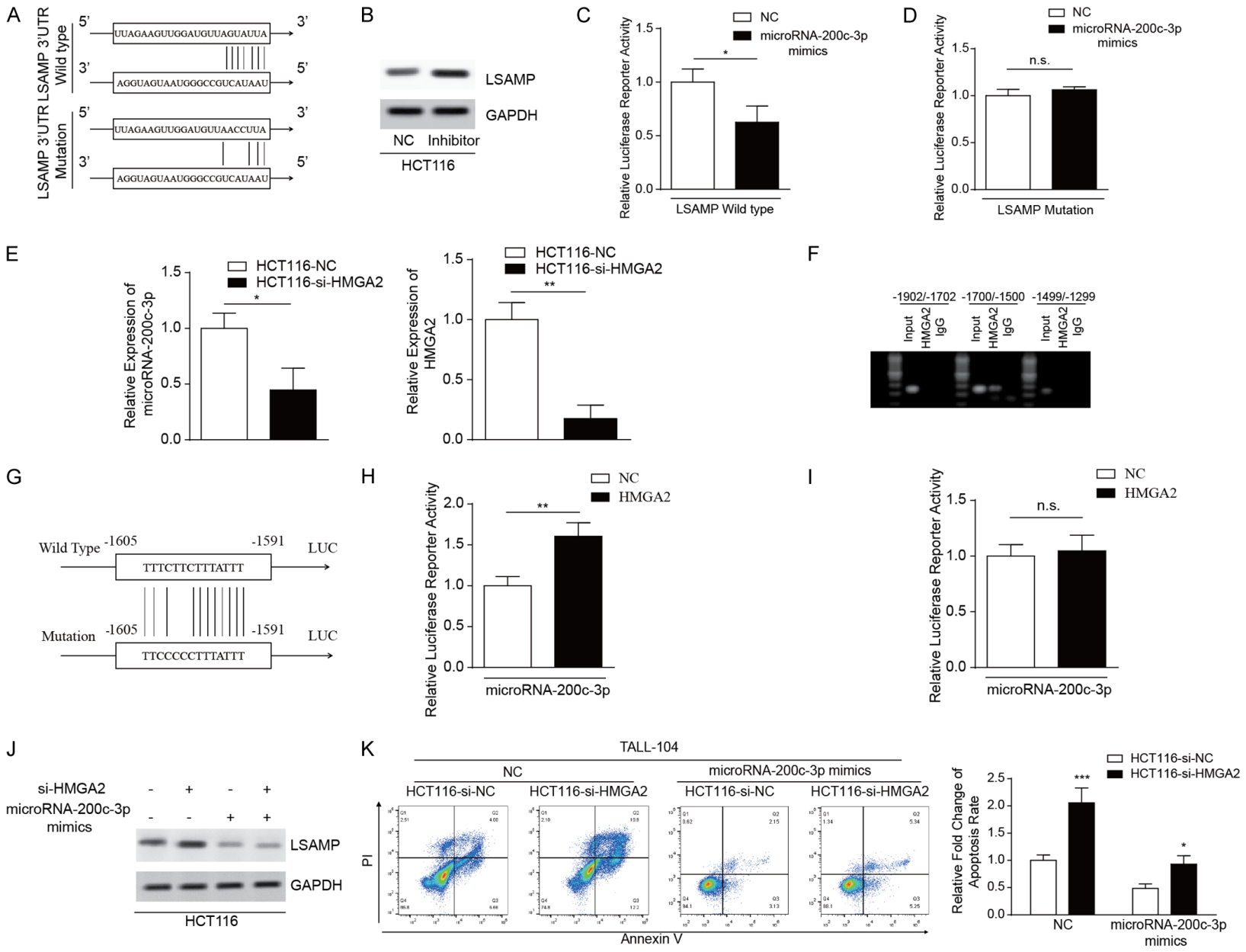
A
LSAMP 3'UTR Wild type
5' UUAGAAGUUGGAUGUUAGUAUUA 3'
3' AGGUAGUAAUGGGCCGUCAUAAU 5'
LSAMP 3'UTR Mutation
5' UUAGAAGUUGGAUGUUAACCUUA 3'
3' AGGUAGUAAUGGGCCGUCAUAAU 5'
B
LSAMP
GAPDH
NC Inhibitor
HCT116
C
NC
microRNA-200c-3p mimics
Relative Luciferase Reporter Activity
LSAMP Wild type
D
NC
microRNA-200c-3p mimics
n.s.
Relative Luciferase Reporter Activity
LSAMP Mutation
E
HCT116-NC
HCT116-si-HMGA2
Relative Expression of microRNA-200c-3p
Relative Expression of HMGA2
F
-1902/-1702 -1700/-1500 -1499/-1299
Input HMGA2 IgG
G
Wild Type -1605 -1591 LUC
TTTCTTCTTTATTT
Mutation -1605 -1591 LUC
TTCCCCCTTTATTT
H
NC
HMGA2
Relative Luciferase Reporter Activity
microRNA-200c-3p
I
NC
HMGA2
n.s.
Relative Luciferase Reporter Activity
microRNA-200c-3p
J
si-HMGA2
microRNA-200c-3p mimics
LSAMP
GAPDH
HCT116
K
TALL-104
NC
microRNA-200c-3p mimics
HCT116-si-NC
HCT116-si-HMGA2
PI
Annexin V
HCT116-si-NC
HCT116-si-HMGA2
Relative Fold Change of Apoptosis Rate
NC
microRNA-200c-3p mimics

Figure 11. Regulation of LSAMP via the HMGA2/miRNA-200c-3p axis. (A) Schematic representation of the wildtype (WT) and mutated luciferase LSAMP 3'-UTR plasmids. (B) Western blotting analysis of LSAMP expression in the indicated cells. Relative luciferase activity of LSAMP in HEK293T cells, in the presence of absence of miRNA-200c-3p overexpression, when transfected with (C) WT or (D) mutant luciferase plasmids. (E) qPCR analysis of the relative expression levels of *HMGA2* and miRNA-200c-3p in the indicated cells. (F) ChIP-PCR analysis were performed using specific primer pairs for the miRNA-200c-3p promoter. (G) Schematic representation of the WT and mutated miRNA-200c-3p promoter within the luciferase plasmids. Relative luciferase activity of microRNA-200c-3p in HEK293T cells in the presence of absence of HMGA2 overexpression when transfected with (H) WT or (I) mutant luciferase plasmids. (J) Western blotting analysis of LSAMP expression in *HMGA2*-depleted or control cells in the presence or absence of miRNA-200c-3p overexpression. (K) Flow cytometry analysis of apoptosis in *HMGA2*-depleted and control cells in the presence or absence of miRNA-200c-3p overexpression and TALL-104 cells. $*P < 0.05$, $**P < 0.01$, $***P < 0.001$.

but not the mutant 3'-UTR of *LSAMP* (**Figure 11C** and **11D**). These results reveal that miRNA-200c-3p specifically inhibited LSAMP expression by directly interacting with the *LSAMP* 3'-UTR.

Many studies have reported that genes encoding transcription factors can regulate the ectopic expression of miRNAs. Therefore, we investigated whether the miRNA-200c-3p expression was regulated by transcription factors. As a member of the High mobility group (HMG) protein family, HMGA2 has been shown to regulate its downstream targets at the transcriptional level by binding to the adenine-thymine (AT)-rich motif, TTCTTTT [16]. We therefore sought to investigate whether HMGA2 could regulate miRNA-200c-3p. Knockdown of *HMGA2* reduced miRNA-200c-3p expression in HCT116 cells (**Figure 11E**). Interestingly, we found a potential HMGA2-targeted AT-rich binding sequence in the -1605/-1591 region of the miRNA-200c-3p promoter. ChIP-PCR analysis further demonstrated that HMGA2 directly bound to the miRNA-200c-3p promoter region of -1700/-1500 (**Figure 11F**). Subsequently, luciferase reporter vectors containing the miRNA-200c-3p promoter or the corresponding point mutant were developed and used in the luciferase reporter assay (**Figure 11G**). The results showed that HMGA2 transactivated miRNA-200c-3p, while mutation of the -1605/-1591 region of the promoter abolished the HMGA2-induced luciferase activity. This finding indicates that the identified sequence on the miRNA-200c-3p promoter was required for the direct binding of HMGA2 (**Figure 11H** and **11I**).

Western blotting subsequently showed that the overexpression of miRNA-200c-3p attenuated the upregulation *LSAMP,* which was induced by *HMGA2* knockdown, suggesting that downregulation of *LSAMP* by *HMGA2* relied on miRNA-200c-3p (**Figure 11J**). Knockdown of *HMGA2* increased sensitivity to $CD8^+$-T-cell-mediated cytotoxicity, an effect which was alleviated by miRNA-200c-3p overexpression (**Figure 11K**). Taken together, these findings suggest that HMGA2 promotes an immunosuppressive phenotype in CRC through the miRNA-200c-3p/LSAMP/Wnt/β-catenin axis.

Discussion

Since CRC is still a leading cause of death worldwide, novel biomarkers and risk evaluation parameters are urgently needed to predict the prognosis and improve the outcome of CRC patients. CRC cells interact and co-evolve with various components of the TME to promote cancer occurrence and development [17]. It has been well documented that the infiltration of immune cells into the TME is closely related to the prognosis of CRC patients [18]. Therefore, some researchers have proposed that the quantification of immune cells in the TME could predict the prognosis of CRC patients; indeed, this is now widely used in the evaluation of CRC patients [19]. In the present study, we identified TME-related genes and developed a TME-associated risk scoring system for CRC prognosis evaluation. High TME-associated risk score was identified as an adverse factor for OS, while a low TME-associated risk score may indicate a better response to immunotherapy and prolonged survival.

Here, we constructed a TME-associated risk score prognostic model using nine genes, which are related to the stromal and immune scores of CRC patients. Among these genes, some had an effect on the TME, which supported the accuracy of our prediction. For example, WW domain-containing transcription regulator 1 (WWTR1, also known as TAZ) acts as the downstream effector of the Hippo signaling

pathway [20]. Rensburg et al. [21] demonstrated that WWTR1 transactivates PD-L1 via the TEAD response element and thereby suppresses the anti-tumor activity of TME. Platelet derived growth factor receptor alpha (PDGFRA) is a tyrosine kinase type III receptor, which is preferentially, highly expressed in cancer-associated fibroblasts rather than pancreatic cancer cells [22]. Patients with PDGFRA-mutant gastrointestinal stromal tumors (GISTs) are enriched in infiltrating immune cells, including $CD3^+$, $CD8^+$, and $CD68^+$ cells. Besides, PDGFRA-mutant GISTs have a much higher density of $CD8^+$ T cells than $FOXP3^+$ T cells, which is associated with a better prognosis [23]. A disintegrin and metalloprotease 8 (ADAM8, also known as CD156) is a transmembrane glycoprotein, which is expressed in macrophages, B lymphocytes, dendritic cells, glial cells, and eosinophils. The knockdown of *ADAM8* in CRC cells also increased the anti-tumor activity of tumor-infiltrating lymphocytes [24]. In addition, CCL22 acts as a chemokine released by tumor-associated macrophages and regulates the activity of T cell [25, 26]. However, although high CCL22 expression was associated with an immunosuppressive TME, CCL22 expression was markedly reduced in the KRAS and APC mutation groups (compared with WT). This indicates that CCL22 has a complex role in CRC tumorigenesis [27]. LAGLS1, also known as Galectin 1, participates in the integration of TGF-β/Snail and TNF-α/NF-κB pathways and promotes the interaction between CRC cells and the stroma [28]. Therefore, genes that have not been intensively studied may provide new targets for evaluating and inhibiting tumorigenesis. In this study, we explored the role of a novel TME-associated risk-score-related gene, *LSAMP*, in CRC oncoimmunology.

LSAMP, which encodes the limbic system associated membrane protein, is located on chromosome 3q13.31. In African American men with prostate cancer, a *LSAMP* deletion correlates with a worse recurrence-free survival [29]. A study of microarray-based comparative genomic hybridization using 36 osteosarcoma tumors and 20 cell lines revealed that *LSAMP* was frequently deleted [30]. *In vitro* and *in vivo* experiments disclosed that the overexpression of LSAMP hindered the proliferation of osteosarcoma or normal osteoblasts. Moreover, a mechanistic study identified several downstream genes, including apoptotic and cell-cycle transcripts, *VEGF receptor 1*, *HES1*, *CTAG2*, and *KLF10* [31, 32]. *LSAMP* with a breakpoint-span of t(1;3)(q32.1;q13.3) is often underexpressed (with a methylated promoter) in clear cell renal cell carcinoma (ccRCC); the overexpression of *LSAMP* inhibits ccRCC proliferation *in vitro* [33]. Consistent with these previous studies, we demonstrated that *LSAMP* was a novel TME-associated risk-related gene, the overexpression of which increased sensitivity to $CD8^+$-T-cell-mediated cytotoxicity.

Many studies have illustrated that Wnt/β-catenin signaling is closely related to immune evasion. For example, Tang et al. [14] showed that FERMT3 attenuated CRC immune evasion by inhibiting Wnt/β-catenin/PD-L1 signaling. In the present study, we demonstrated that LSAMP increased the transcriptional activity of the canonical Wnt reporter and inhibited the nuclear localization of β-catenin. Rescue experiments showed that SKL2001 alleviated the LSAMP-induced sensitivity to $CD8^+$-T-cell-mediated cytotoxicity. Thus, we concluded that LSAMP rendered CRC cells more sensitive to $CD8^+$-T-cell-mediated killing by inhibiting Wnt/β-catenin signaling.

miRNAs and transcription factors are also involved in tumorigenesis [34, 35]. For instance, binding of miRNA-200c to *ZEB2* downregulates its expression, thereby suppressing cancer metastasis [36, 37]. In addition, although miRNA-200c alleviates the multidrug resistance and metastasis of CRC [38], its overexpression was also demonstrated to promote the proliferation of CRC cells [39]. This indicates that miRNA-200 has a dual role in CRC tumorigenesis. In the present study, we demonstrated that miRNA-200c-3p suppressed LSAMP expression via direct interaction with its 3'-UTR. Additionally, we identified a potential AT-rich binding sequence of the transcription factor HMGA2 on the miRNA-200c-3p promoter. The dual luciferase reporter assay and qPCR further demonstrated that HMGA2 regulated miRNA-200c-3p via transactivation. HMGA2 is associated with a series of oncological behaviors including tumor cell invasion, metastasis, proliferation, and chemoresistance [40-42]. A recent study showed that HMGA2 promoted CRC progression via the M2 polarization of tumor-associated macrophages, which

indicates that HMGA2 plays an immune-suppressive role [43]. In the present study, we demonstrated that HMGA2 reduced the sensitivity of CRC cells to $CD8^+$-T-cell-mediated cytotoxicity via the miRNA-200c-3p/LSAMP/Wnt axis.

The strength of our study lies in the construction of the TME-associated risk score model, which identified several candidate genes and suggested that LSAMP acted as a potential novel biomarker. Furthermore, we assessed the biological role of LSAMP and showed that the HMGA2/miRNA-200c-3p/LSAMP/Wnt axis was involved in the immune response to CRC. Our study highlights the value of novel immune-related factors in CRC. Moreover, the methods used to detect these biomarkers may provide novel strategies for improving the response of patients with CRC to immunotherapy and ultimately their prognosis.

The present study has several limitations. We focused on validating the biological and clinical significance of *LSAMP*. Thus, validation of the other TME-associated risk-related genes is needed. In addition, although we analyzed the mutation status of CRC patients with different TME-associated risk scores and identified ten high-mutation-frequency genes, the involvement of these genes in the LSAMP-mediated immune response to CRC has not been investigated. Therefore, further studies are needed to improve our understanding of the mechanisms underlying CRC progression.

Conclusions

In conclusion, we constructed a TME-associated risk score model to predict the prognosis of CRC patients. We identified *LSAMP* as a novel TME-associated-risk-score-related gene in CRC. Functional validation and mechanistic study revealed that the HMGA2/miRNA-200c-3p/LSAMP/Wnt axis was immunological factor in CRC patients. Therefore, our study highlights the role of the HMGA2/miRNA-200c-3p/LSAMP/Wnt axis in CRC immunology, which may provide a new strategy for improving the immunotherapeutic response of CRC patients.

Acknowledgements

We thank Charlesworth Author Services for the English language editing of the article. This work was supported by the National Natural Science Foundation of China (grant number: 82103334), Zhejiang Provincial Natural Science Foundation of China (grant number: LQ21H160009) and Zhejiang Medical and Health Science and Technology Plan (2021-KY409).

Informed written consent was obtained from all participants.

Disclosure of conflict of interest

None.

Address correspondence to: Zejun Fang, Central Laboratory, Sanmen People's Hospital of Zhejiang Province, Sanmenwan Branch of The First Affiliated Hospital, College of Medicine, Zhejiang University, Sanmen 317100, Zhejiang, China. Tel: +86-576-83361583; Fax: +86-576-83361583; E-mail: fangzejun@zjsmyy.com

References

[1] Siegel RL, Miller KD, Goding Sauer A, Fedewa SA, Butterly LF, Anderson JC, Cercek A, Smith RA and Jemal A. Colorectal cancer statistics, 2020. CA Cancer J Clin 2020; 70: 145-164.

[2] Alyabsi M, Sabatin F, Ramadan M and Jazieh AR. Colorectal cancer survival among ministry of national guard-health affairs (MNG-HA) population 2009-2017: retrospective study. BMC Cancer 2021; 21: 954.

[3] Binnewies M, Roberts EW, Kersten K, Chan V, Fearon DF, Merad M, Coussens LM, Gabrilovich DI, Ostrand-Rosenberg S, Hedrick CC, Vonderheide RH, Pittet MJ, Jain RK, Zou W, Howcroft TK, Woodhouse EC, Weinberg RA and Krummel MF. Understanding the tumor immune microenvironment (TIME) for effective therapy. Nat Med 2018; 24: 541-550.

[4] Giraldo NA, Becht E, Vano Y, Petitprez F, Lacroix L, Validire P, Sanchez-Salas R, Ingels A, Oudard S, Moatti A, Buttard B, Bourass S, Germain C, Cathelineau X, Fridman WH and Sautes-Fridman C. Tumor-infiltrating and peripheral blood T-cell immunophenotypes predict early relapse in localized clear cell renal cell carcinoma. Clin Cancer Res 2017; 23: 4416-4428.

[5] Denton AE, Roberts EW and Fearon DT. Stromal cells in the tumor microenvironment. Adv Exp Med Biol 2018; 1060: 99-114.

[6] Jun X, Gao S, Yu L and Wang G. The clinical relevance and prediction efficacy from therapy of tumor microenvironment related signature score in colorectal cancer. Front Oncol 2023; 13: 1123455.

[7] Shi L, Zhang Y and Wang H. Prognostic prediction based on histopathologic features of tumor microenvironment in colorectal cancer. Front Med (Lausanne) 2023; 10: 1154077.
[8] Wu X, Li J, Zhang Y, Cheng Y, Wu Z, Zhan W and Deng Y. Identification of immune cell infiltration landscape for predicting prognosis of colorectal cancer. Gastroenterol Rep (Oxf) 2023; 11: goad014.
[9] Thorsson V, Gibbs DL, Brown SD, Wolf D, Bortone DS, Ou Yang TH, Porta-Pardo E, Gao GF, Plaisier CL, Eddy JA, Ziv E, Culhane AC, Paull EO, Sivakumar IKA, Gentles AJ, Malhotra R, Farshidfar F, Colaprico A, Parker JS, Mose LE, Vo NS, Liu J, Liu Y, Rader J, Dhankani V, Reynolds SM, Bowlby R, Califano A, Cherniack AD, Anastassiou D, Bedognetti D, Mokrab Y, Newman AM, Rao A, Chen K, Krasnitz A, Hu H, Malta TM, Noushmehr H, Pedamallu CS, Bullman S, Ojesina AI, Lamb A, Zhou W, Shen H, Choueiri TK, Weinstein JN, Guinney J, Saltz J, Holt RA, Rabkin CS; Cancer Genome Atlas Research Network; Lazar AJ, Serody JS, Demicco EG, Disis ML, Vincent BG and Shmulevich I. The immune landscape of cancer. Immunity 2018; 48: 812-830, e814.
[10] Xu X, Gong C, Wang Y, Hu Y, Liu H and Fang Z. Multi-omics analysis to identify driving factors in colorectal cancer. Epigenomics 2020; 12: 1633-1650.
[11] Yuan Q, Zhang W and Shang W. Identification and validation of a prognostic risk-scoring model based on sphingolipid metabolism-associated cluster in colon adenocarcinoma. Front Endocrinol (Lausanne) 2022; 13: 1045167.
[12] Zhao H, Ming T, Tang S, Ren S, Yang H, Liu M, Tao Q and Xu H. Wnt signaling in colorectal cancer: pathogenic role and therapeutic target. Mol Cancer 2022; 21: 144.
[13] Zhang L, Ren CF, Yang Z, Gong LB, Wang C, Feng M and Guan WX. Forkhead Box S1 mediates epithelial-mesenchymal transition through the Wnt/beta-catenin signaling pathway to regulate colorectal cancer progression. J Transl Med 2022; 20: 327.
[14] Tang Y, Nan N, Gui C, Zhou X, Jiang W and Zhou X. Blockage of PD-L1 by FERMT3-mediated Wnt/beta-catenin signalling regulates chemoresistance and immune evasion of colorectal cancer cells. Clin Exp Pharmacol Physiol 2022; 49: 988-997.
[15] Li J, Ji Y, Chen N, Wang H, Fang C, Yin X, Jiang Z, Dong Z, Zhu D, Fu J, Zhou W, Jiang R, He L, Hantao Z, Shi G, Cheng L, Su X, Dai L and Deng H. A specific upregulated long noncoding RNA in colorectal cancer promotes cancer progression. JCI Insight 2022; 7: e158855.
[16] Li Y, Zhao Z, Xu C, Zhou Z, Zhu Z and You T. HMGA2 induces transcription factor Slug expression to promote epithelial-to-mesenchymal transition and contributes to colon cancer progression. Cancer Lett 2014; 355: 130-140.
[17] Zafari N, Khosravi F, Rezaee Z, Esfandyari S, Bahiraei M, Bahramy A, Ferns GA and Avan A. The role of the tumor microenvironment in colorectal cancer and the potential therapeutic approaches. J Clin Lab Anal 2022; 36: e24585.
[18] Galon J, Fridman WH and Pages F. The adaptive immunologic microenvironment in colorectal cancer: a novel perspective. Cancer Res 2007; 67: 1883-1886.
[19] Mlecnik B, Bindea G, Angell HK, Maby P, Angelova M, Tougeron D, Church SE, Lafontaine L, Fischer M, Fredriksen T, Sasso M, Bilocq AM, Kirilovsky A, Obenauf AC, Hamieh M, Berger A, Bruneval P, Tuech JJ, Sabourin JC, Le Pessot F, Mauillon J, Rafii A, Laurent-Puig P, Speicher MR, Trajanoski Z, Michel P, Sesboue R, Frebourg T, Pages F, Valge-Archer V, Latouche JB and Galon J. Integrative analyses of colorectal cancer show immunoscore is a stronger predictor of patient survival than microsatellite instability. Immunity 2016; 44: 698-711.
[20] Thompson BJ. YAP/TAZ: drivers of tumor growth, metastasis, and resistance to therapy. Bioessays 2020; 42: e1900162.
[21] Janse van Rensburg HJ, Azad T, Ling M, Hao Y, Snetsinger B, Khanal P, Minassian LM, Graham CH, Rauh MJ and Yang X. The hippo pathway component TAZ promotes immune evasion in human cancer through PD-L1. Cancer Res 2018; 78: 1457-1470.
[22] Wu Z, Xu J, Tang R, Wang W, Zhang B, Yu X, Liu J and Shi S. The role of PDGFRA in predicting oncological and immune characteristics in pancreatic ductal adenocarcinoma. J Oncol 2022; 2022: 4148805.
[23] Sun X, Sun J, Yuan W, Gao X, Fu M, Xue A, Li H, Shu P, Fang Y, Hou Y, Shen K, Sun Y, Qin J and Qin X. Immune cell infiltration and the expression of PD-1 and PD-L1 in primary PDGFRA-mutant gastrointestinal stromal tumors. J Gastrointest Surg 2021; 25: 2091-2100.
[24] Liao R, Ma QZ, Zhou CY, Li JJ, Weng NN, Yang Y and Zhu Q. Identification of biomarkers related to tumor-infiltrating lymphocytes (TILs) infiltration with gene co-expression network in colorectal cancer. Bioengineered 2021; 12: 1676-1688.
[25] Mantovani A, Gray PA, Van Damme J and Sozzani S. Macrophage-derived chemokine (MDC). J Leukoc Biol 2000; 68: 400-404.
[26] Lecoq I, Kopp KL, Chapellier M, Mantas P, Martinenaite E, Perez-Penco M, Ronn Olsen L, Zocca MB, Wakatsuki Pedersen A and Andersen MH. CCL22-based peptide vaccines induce anti-cancer immunity by modulating tumor mi-

croenvironment. Oncoimmunology 2022; 11: 2115655.
[27] Wang H, Luo K, Guan Z, Li Z, Xiang J, Ou S, Tao Y, Ran S, Ye J, Ma T, Qiao T, Zhang Z, Jin Y, Song Y and Huang R. Identification of the crucial role of CCL22 in F. nucleatum-related colorectal tumorigenesis that correlates with tumor microenvironment and immune checkpoint therapy. Front Genet 2022; 13: 811900.
[28] Li H, Zhong A, Li S, Meng X, Wang X, Xu F and Lai M. The integrated pathway of TGFbeta/Snail with TNFalpha/NFkappaB may facilitate the tumor-stroma interaction in the EMT process and colorectal cancer prognosis. Sci Rep 2017; 7: 4915.
[29] Petrovics G, Li H, Stumpel T, Tan SH, Young D, Katta S, Li Q, Ying K, Klocke B, Ravindranath L, Kohaar I, Chen Y, Ribli D, Grote K, Zou H, Cheng J, Dalgard CL, Zhang S, Csabai I, Kagan J, Takeda D, Loda M, Srivastava S, Scherf M, Seifert M, Gaiser T, McLeod DG, Szallasi Z, Ebner R, Werner T, Sesterhenn IA, Freedman M, Dobi A and Srivastava S. A novel genomic alteration of LSAMP associates with aggressive prostate cancer in African American men. EBioMedicine 2015; 2: 1957-1964.
[30] Kresse SH, Ohnstad HO, Paulsen EB, Bjerkehagen B, Szuhai K, Serra M, Schaefer KL, Myklebost O and Meza-Zepeda LA. LSAMP, a novel candidate tumor suppressor gene in human osteosarcomas, identified by array comparative genomic hybridization. Genes Chromosomes Cancer 2009; 48: 679-693.
[31] Baroy T, Kresse SH, Skarn M, Stabell M, Castro R, Lauvrak S, Llombart-Bosch A, Myklebost O and Meza-Zepeda LA. Reexpression of LSAMP inhibits tumor growth in a preclinical osteosarcoma model. Mol Cancer 2014; 13: 93.
[32] Pasic I, Shlien A, Durbin AD, Stavropoulos DJ, Baskin B, Ray PN, Novokmet A and Malkin D. Recurrent focal copy-number changes and loss of heterozygosity implicate two noncoding RNAs and one tumor suppressor gene at chromosome 3q13.31 in osteosarcoma. Cancer Res 2010; 70: 160-171.
[33] Chen J, Lui WO, Vos MD, Clark GJ, Takahashi M, Schoumans J, Khoo SK, Petillo D, Lavery T, Sugimura J, Astuti D, Zhang C, Kagawa S, Maher ER, Larsson C, Alberts AS, Kanayama HO and Teh BT. The t(1;3) breakpoint-spanning genes LSAMP and NORE1 are involved in clear cell renal cell carcinomas. Cancer Cell 2003; 4: 405-413.
[34] Hu H, Zhang Q, Hu FF, Liu CJ and Guo AY. A comprehensive survey for human transcription factors on expression, regulation, interaction, phenotype and cancer survival. Brief Bioinform 2021; 22: bbab002.
[35] de Rooij LA, Mastebroek DJ, Ten Voorde N, van der Wall E, van Diest PJ and Moelans CB. The microRNA lifecycle in health and cancer. Cancers (Basel) 2022; 14: 5748.
[36] Li H, Xu L, Li C, Zhao L, Ma Y, Zheng H, Li Z, Zhang Y, Wang R, Liu Y and Qu X. Ubiquitin ligase Cbl-b represses IGF-I-induced epithelial mesenchymal transition via ZEB2 and microRNA-200c regulation in gastric cancer cells. Mol Cancer 2014; 13: 136.
[37] Zhang J, Zhang H, Qin Y, Chen C, Yang J, Song N and Gu M. MicroRNA-200c-3p/ZEB2 loop plays a crucial role in the tumor progression of prostate carcinoma. Ann Transl Med 2019; 7: 141.
[38] Sui H, Cai GX, Pan SF, Deng WL, Wang YW, Chen ZS, Cai SJ, Zhu HR and Li Q. miR200c attenuates P-gp-mediated MDR and metastasis by targeting JNK2/c-Jun signaling pathway in colorectal cancer. Mol Cancer Ther 2014; 13: 3137-3151.
[39] Pan Y, Liang H, Chen W, Zhang H, Wang N, Wang F, Zhang S, Liu Y, Zhao C, Yan X, Zhang J, Zhang CY, Gu H, Zen K and Chen X. microRNA-200b and microRNA-200c promote colorectal cancer cell proliferation via targeting the reversion-inducing cysteine-rich protein with Kazal motifs. RNA Biol 2015; 12: 276-289.
[40] Deng X, Kong F, Li S, Jiang H, Dong L, Xu X, Zhang X, Yuan H, Xu Y, Chu Y, Peng H and Guan M. A KLF4/PiHL/EZH2/HMGA2 regulatory axis and its function in promoting oxaliplatin-resistance of colorectal cancer. Cell Death Dis 2021; 12: 485.
[41] Xu X, Wang Y, Deng H, Liu C, Wu J and Lai M. HMGA2 enhances 5-fluorouracil chemoresistance in colorectal cancer via the Dvl2/Wnt pathway. Oncotarget 2018; 9: 9963-9974.
[42] Wu J, Wang Y, Xu X, Cao H, Sahengbieke S, Sheng H, Huang Q and Lai M. Transcriptional activation of FN1 and IL11 by HMGA2 promotes the malignant behavior of colorectal cancer. Carcinogenesis 2016; 37: 511-521.
[43] Wang X, Wang J, Zhao J, Wang H, Chen J and Wu J. HMGA2 facilitates colorectal cancer progression via STAT3-mediated tumor-associated macrophage recruitment. Theranostics 2022; 12: 963-975.

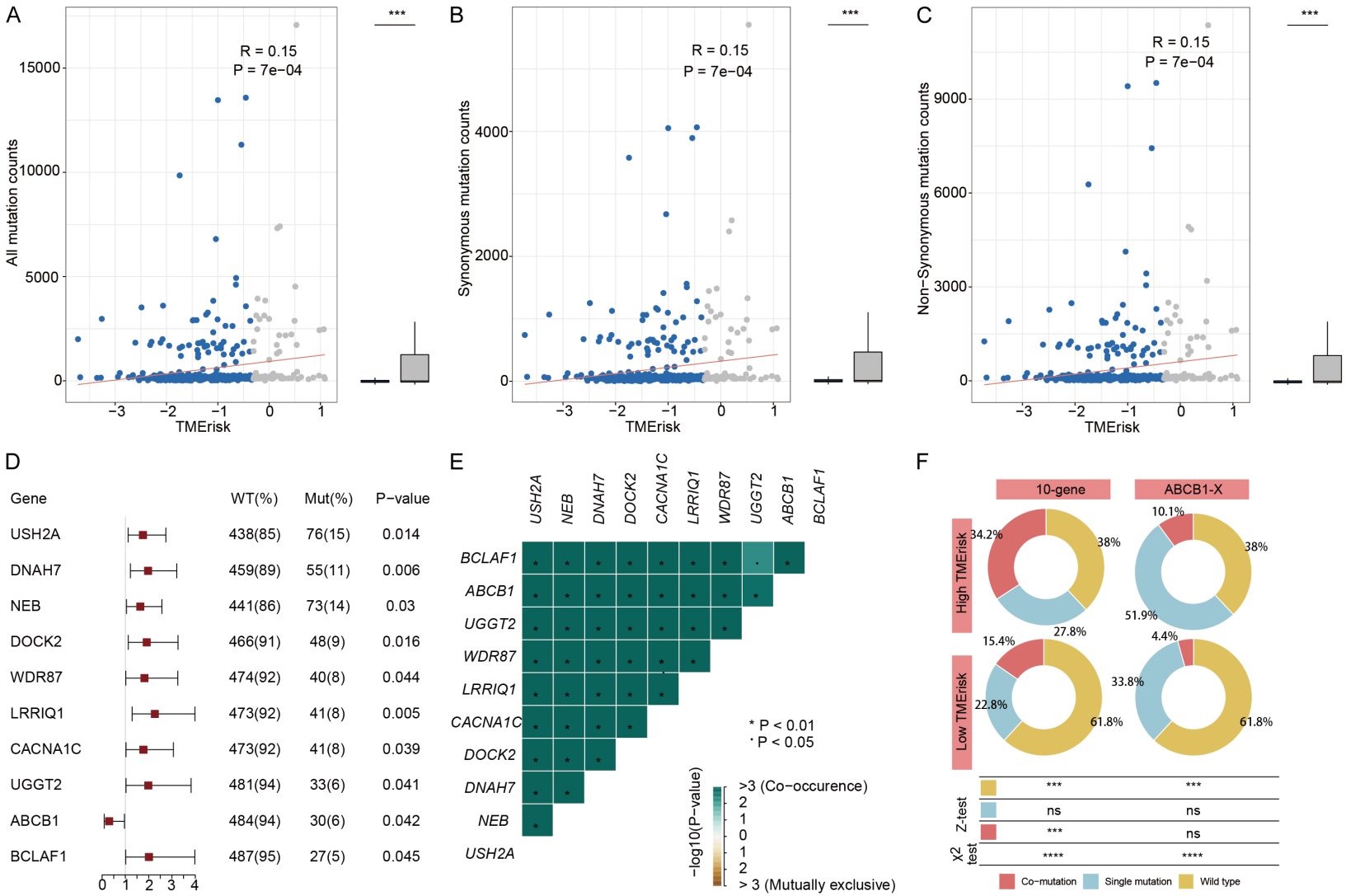

Supplementary Figure 1. Mutation status of CRC patients in the high and low TME-associated risk score groups. Association between the TME-associated risk score and (A) all mutation counts, (B) synonymous mutation counts, and (C) non-synonymous mutation counts. (D) Forest plot of differentially mutated genes between the low and high TME-associated risk groups. (E) Interactions between differentially mutated genes. (F) Assessment of WT, single mutations, and co-mutations within the ten genes (left panel) and *ABCB1 - X* (right panel), where *X* represents the other nine genes. ***$P < 0.001$, ****$P < 0.0001$.